Dry Plasma Reduction to Supported Platinum Nanoparticles for Flexible Dye-sensitized Solar Cells

*Van-Duong Dao[a], Chinh Quoc Tran[a], Seung-Hyeon Ko[b], Ho-Suk Choi[a]**

[a]Department of Chemical Engineering, Chungnam National University, 220 Gung-Dong, Yuseong-Gu, Daejeon 305-764, Korea

[b]Center for Nanoscale Science and Technology, National Institute of Standards and Technology, Gaithersburg, MD 20899.; Institute for Research in Electronics and Applied Physics, University of Maryland, College Park, MD 20742.

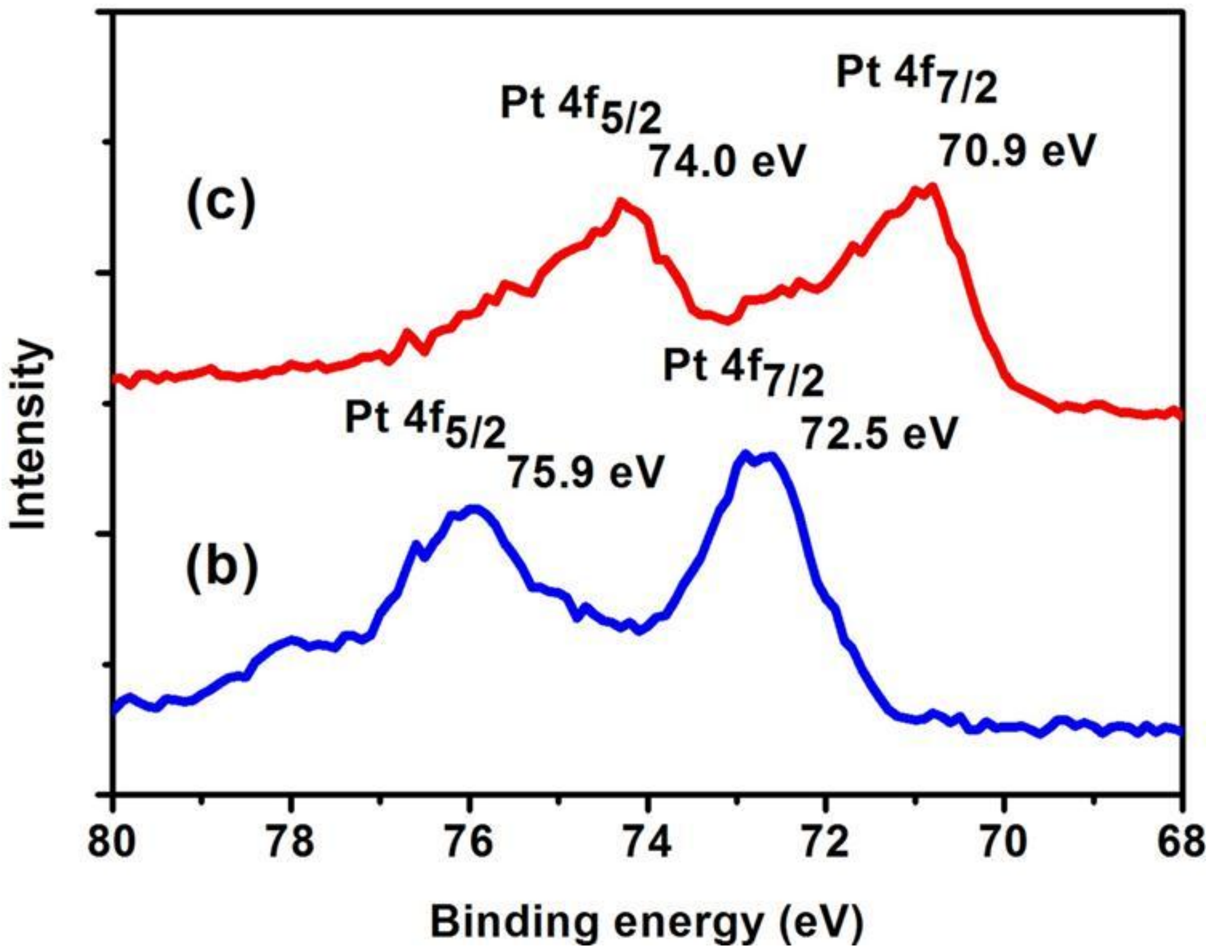

Figure S1. XPS spectra of sample (b), and sample (c), respectively, in Fig. 1.

Table S1. Percentage of elemental composition on the surface of FTO glass.

	Elemental Composition (%)			
Sample	Sn	O	Pt	Cl
(b)	14.55	25.6	15.73	44.12
(c)	31.65	54.88	13.47	0

(b) Before plasma reduction; (c) after plasma reduction

Fig. S1 shows the XPS spectra of FTO glass (b) after drying solvent, and (c) after DPR under pre-optimized conditions. Table S1 represents the elemental composition on the surface of the two samples of (b) and (c).

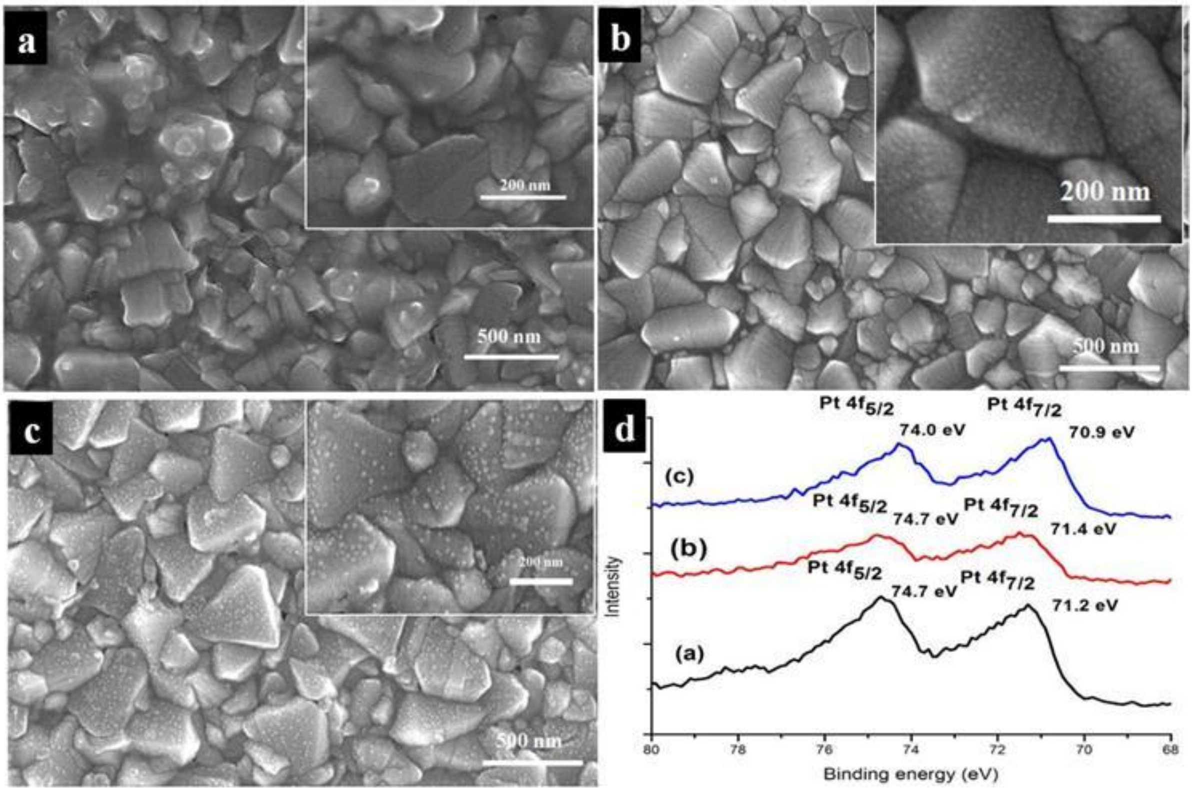

Figure S2. HRSEM images of Pt-NPs on FTO glass substrates treated for (a) 1 min, (b) 5 min, and (c) 15 min. The precursor solution has the $H_2PtCl_6.xH_2O$ concentration of10 mM. Other plasma treatment conditions include the power of 150 W, the Ar flow rate of 5 lpm, and the substrate moving speed of 5 mm/s. (d) XPS spectra of samples of (a), (b), and (c).

Table S2. Percentage of elemental composition on the surface of FTO glass.

Sample	Elemental Composition (%)			
	Sn	O	Pt	Cl
(a)	12.80	68.43	9.77	9.00
(b)	13.02	76.07	5.44	5.46
(c)	31.65	54.88	13.47	0

Table S3. Change of atomic ratio during plasma reducion.

Time Reduction	Cl/Sn	Pt/Sn	Cl/Pt	O/Sn
0	3.03	1.08	2.8	1.7
1	0.70	0.76	0.9	5.3
5	0.42	0.42	1.0	5.8
15	0	0.42	0	1.7

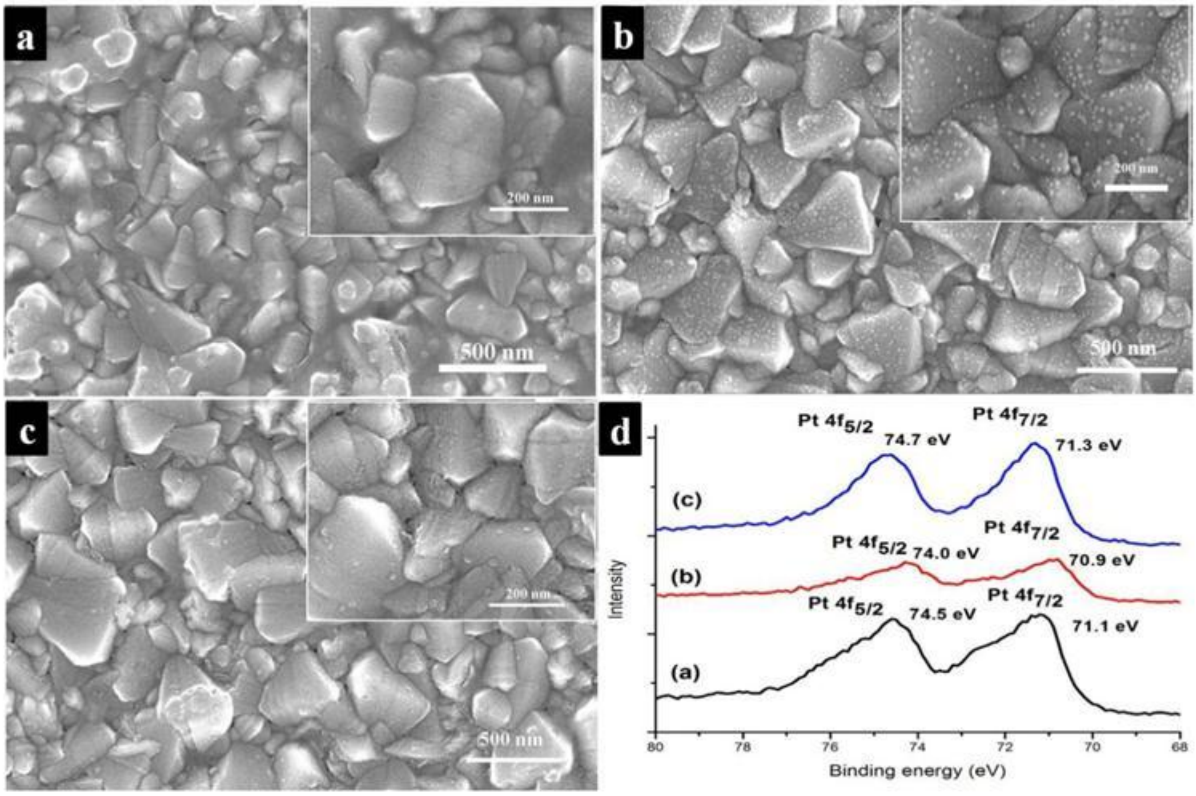

Figure S3. HRSEM images of Pt-NPs on FTO glass substrates treated at the powers of (a) 100 W, (b) 150 W, and (c) 200 W. The precursor solution has the $H_2PtCl_6.xH_2O$ concentration of 10 mM. Other plasma treatment conditions include the treatment time of 15 min, the Ar flow rate of 5 lpm, and the substrate moving speed of 5 mm/s. (d) XPS spectra of samples (a), (b), and (c).

Table S4. Percentage of elemental composition on the surface of FTO glass.

Sample	Elemental Composition (%)			
	Sn	O	Pt	Cl
(a)	12.12	51.93	19.48	16.47
(b)	31.65	54.88	13.47	0
(c)	16.71	58.15	14.93	10.2

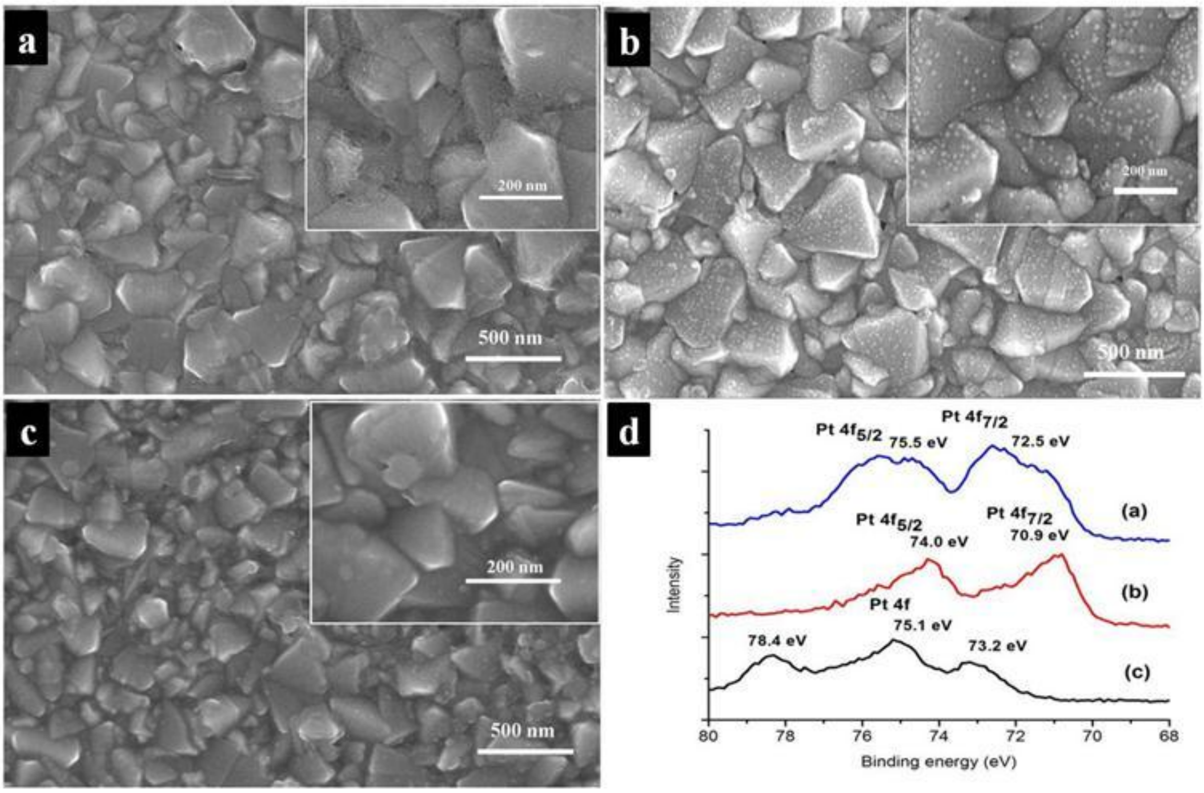

Figure S4. HRSEM images of Pt-NPs on FTO glass substrates treated at the Ar flow rates of (a) 2 lpm, (b) 5 lpm, and (c) 7 lpm. The precursor solution has the $H_2PtCl_6.xH_2O$ concentration of 10 mM. Other plasma treatment conditions include the treatment time of 15 min, the power of 150 W, and the substrate moving speed of 5 mm/s. (d) XPS spectra of samples (a), (b), and (c).

Table S5. Percentage of elemental composition on the surface of FTO glass.

Sample	Elemental Composition (%)			
	Sn	O	Pt	Cl
(a)	9.85	69.63	8.65	11.86
(b)	31.65	54.88	13.47	0
(c)	45.21	18.2	12.4	24.16

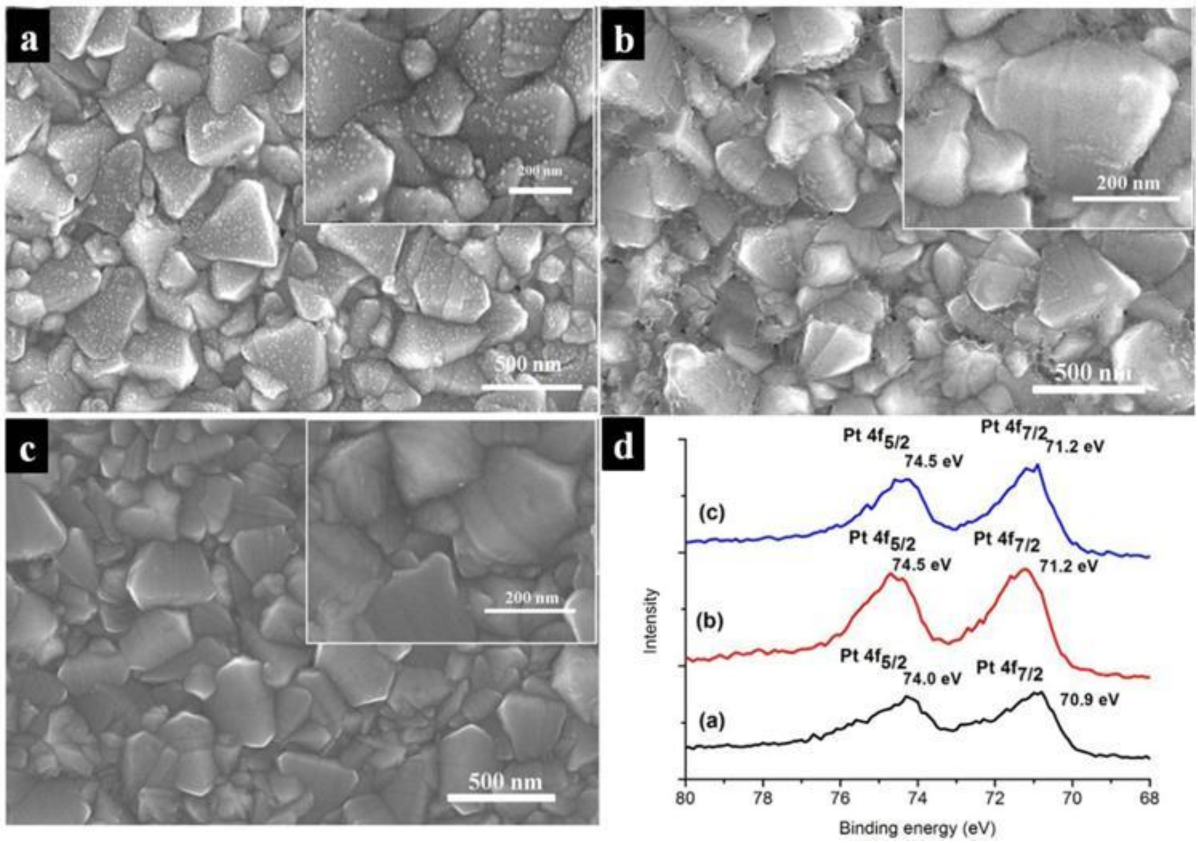

Figure S5. HRSEM images of Pt-NPs on FTO-glass substrate treated at the moving speeds of (a) 5 mm/s, (b) 10 mm/s, and (c) 15 mm/s. The precursor solution has the $H_2PtCl_6.xH_2O$ concentration of 10 mM. Other plasma treatment conditions include the treatment time of 15 min, the power of 150 W, and the Ar flow rate of 5 lpm. (d) XPS spectra of samples (a), (b), and (c).

Table S6. Percentage of elemental composition on the surface of FTO glass.

Sample	Elemental Composition (%)			
	Sn	O	Pt	Cl
(a)	31.65	54.88	13.47	0
(b)	21.53	68.17	5.61	4.68
(c)	18.01	59.48	9.67	12.84

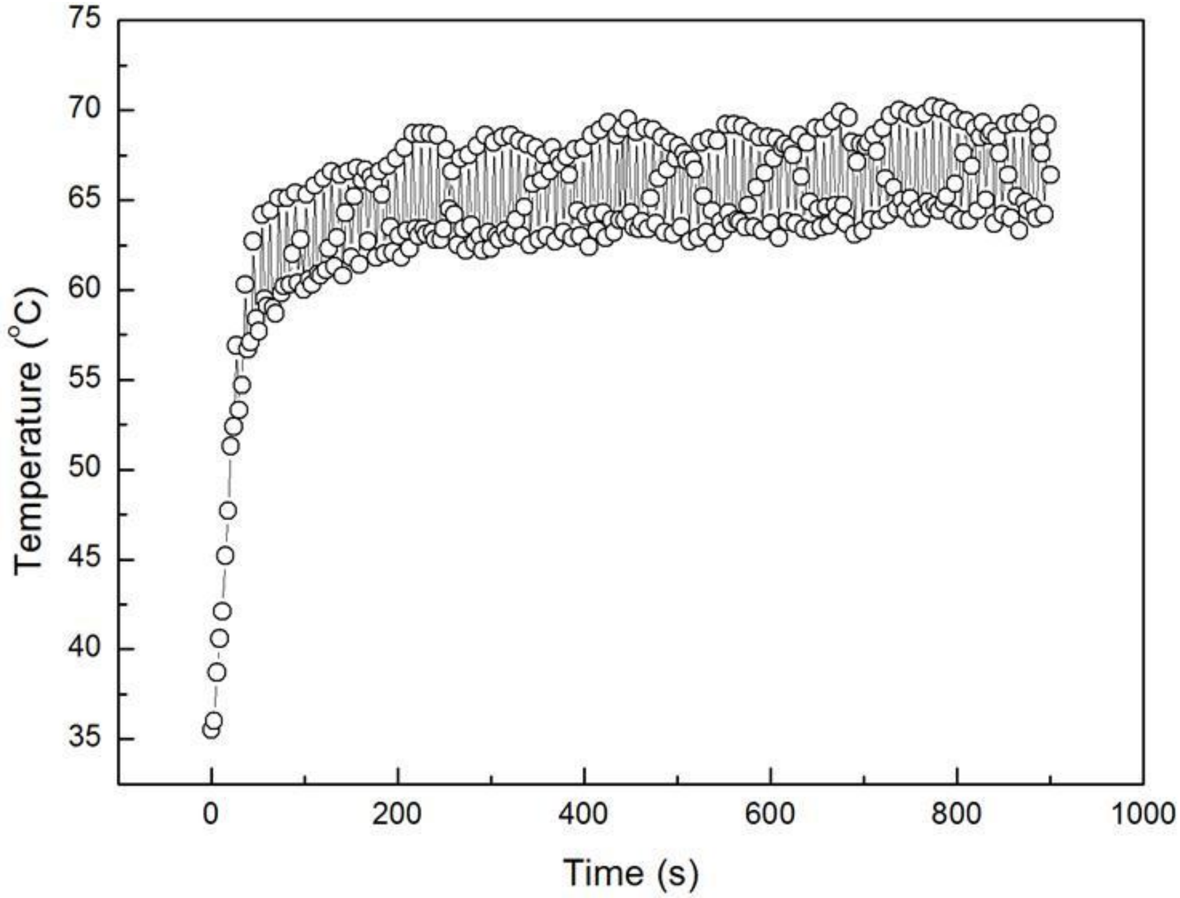

Figure S6. Change of temperature on the surface of FTO glass substrate during plasma reduction.

The temperature on the surface of FTO glass during plasma reduction was measured with a temperature measuring device (Testo 175). Temperature increased over 60°C within 60 sec and then fluctuated at the temperature between 60 °C and 70 °C. The substrate moving speed was 5 mm/s.

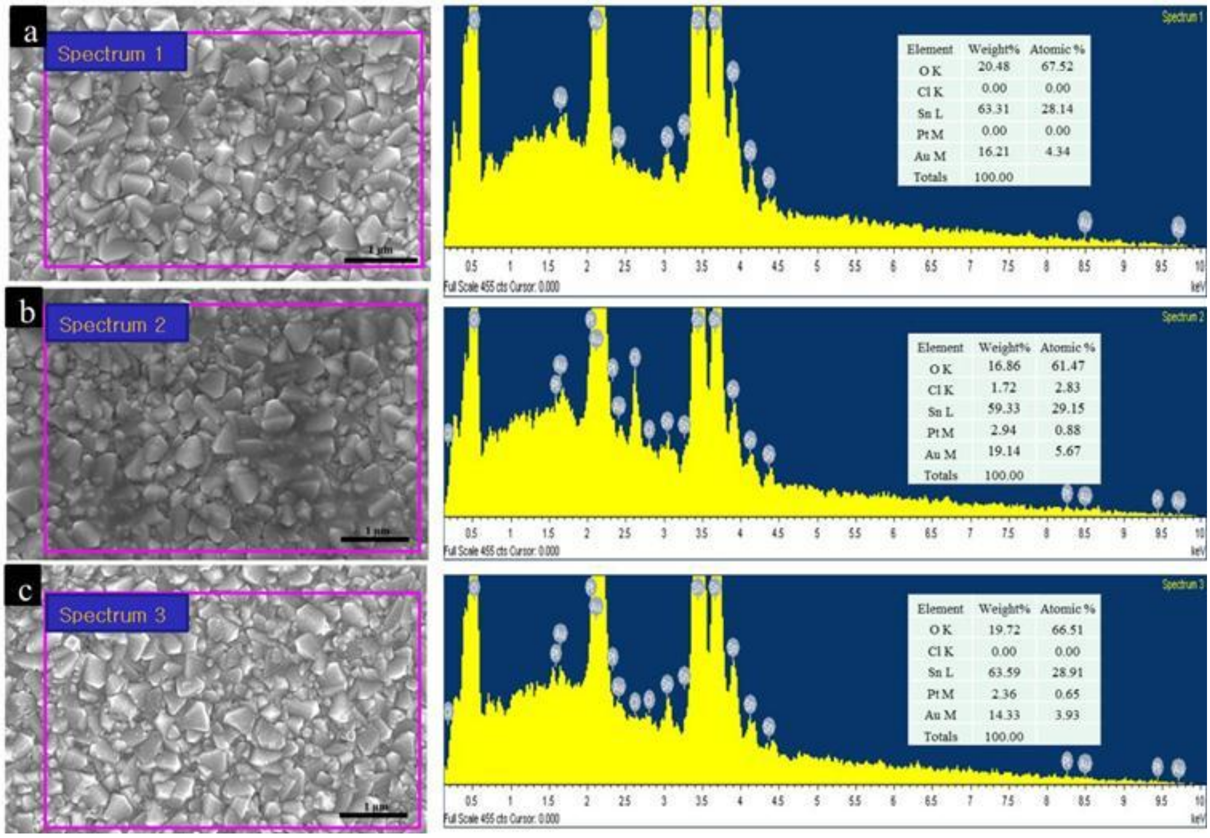

Figure S7. SEM and EDX spectrum of (a) bare FTO glass, (b) FTO glass after dropping H_2PtCl_6 solution and drying solvent, and (c) FTO glass after reducing H_2PtCl_6 with Ar plasma for 15 min.

The physiochemical conversion of H_2PtCl_6 into metallic Pt was further confirmed by energy dispersive spectroscopy (EDX) as shown in Fig. S7. No Pt and Cl were observed on the EDX of bare FTO glass substrate. However, Pt and Cl peaks were observed when H_2PtCl_6 solution was drop-coated on FTO glass substrate. After DPR, the Cl peak was completely removed from the EDX spectrum. The other peaks of Sn, O, and Au in EDX originated from the FTO glass substrate and the coated Au. Hence, H_2PtCl_6 was completely converted into metallic Pt through the DPR process. It also confirmed that Pt-NPs became completely crystallized.

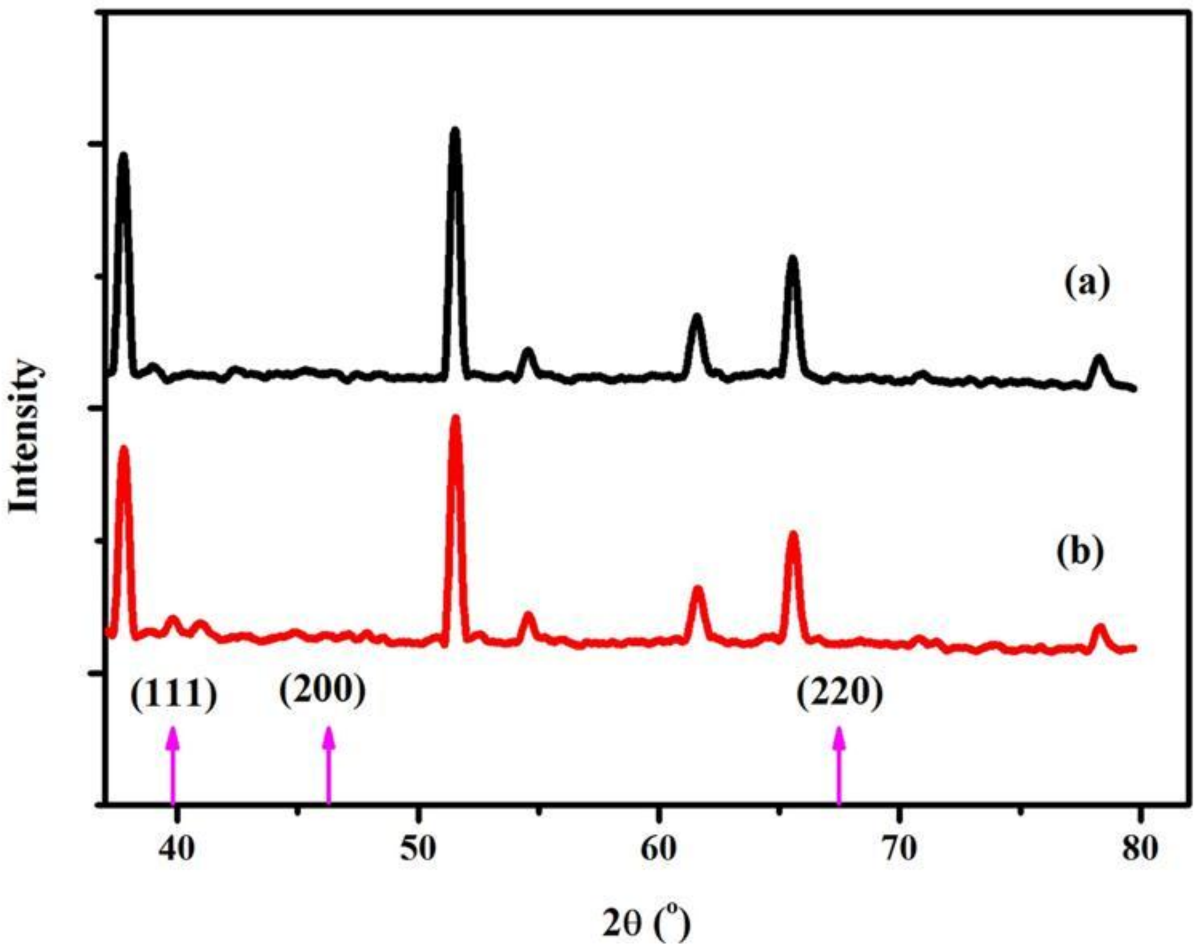

Figure S8. XRD patterns of FTO glass surface drop-coated with H_2PtCl_6 precursor solution (a) before, and (b) after plasma reduction under one atmospheric pressure.

A Rigaku D/MAX-RC (12kW) diffractor with CuK_{α} irradiation was used for the measurements of X-ray diffraction patterns of the samples before and after plasma treatment. Figure S8 shows the XRD patterns of FTO glass substrate drop-coated with H_2PtCl_6 precursor solution before and after plasma reduction under one atmospheric pressure. It can be clearly seen that the diffraction peak of (111) Pt crystal planewas observedin the XRD pattern of (b), although no other peaks at (200) and (220) were observed. Even in the XRD pattern of (a), however, no peaks of (111) Pt crystal planewere observed. This can be further evidence of Pt-NPs formed through plasma reduction under atmospheric pressure.

Table S7. Weight measured at each process for confirming the "Pt missing".

Sample #	Sample description	Weight (μg)
1	Initial FTO glass	2243470
2	FTO glass after plasma pretreatment	2243470
3	FTO glass after dropping 8 μl of Pt precursor solution and completely drying solvent at 70°C for 10min	2243530
4	FTO glass after plasma reduction of Pt precursor	2243480

Amount of plasma etching = 2243470 - 2243470 = 0 (μg)

Amount of Pt precursor salt on FTO glass = 2243530-2243470 = 60 (μg)

Amount of Pt NPs after DPR = 2243480 - 2243470 = 10 (μg)

Amount of Pt metal from 8 μl of Pt precursor solution

= (0.01(M)x0.000008 (l))x409.8(mole/g)x195 (mole/g)/409.8(mole/g) = 15.6 (μg)

Since the amount of "Pt missing" after DPR was estimated as 5.6 μg, there must be some loss of Pt during DPR.

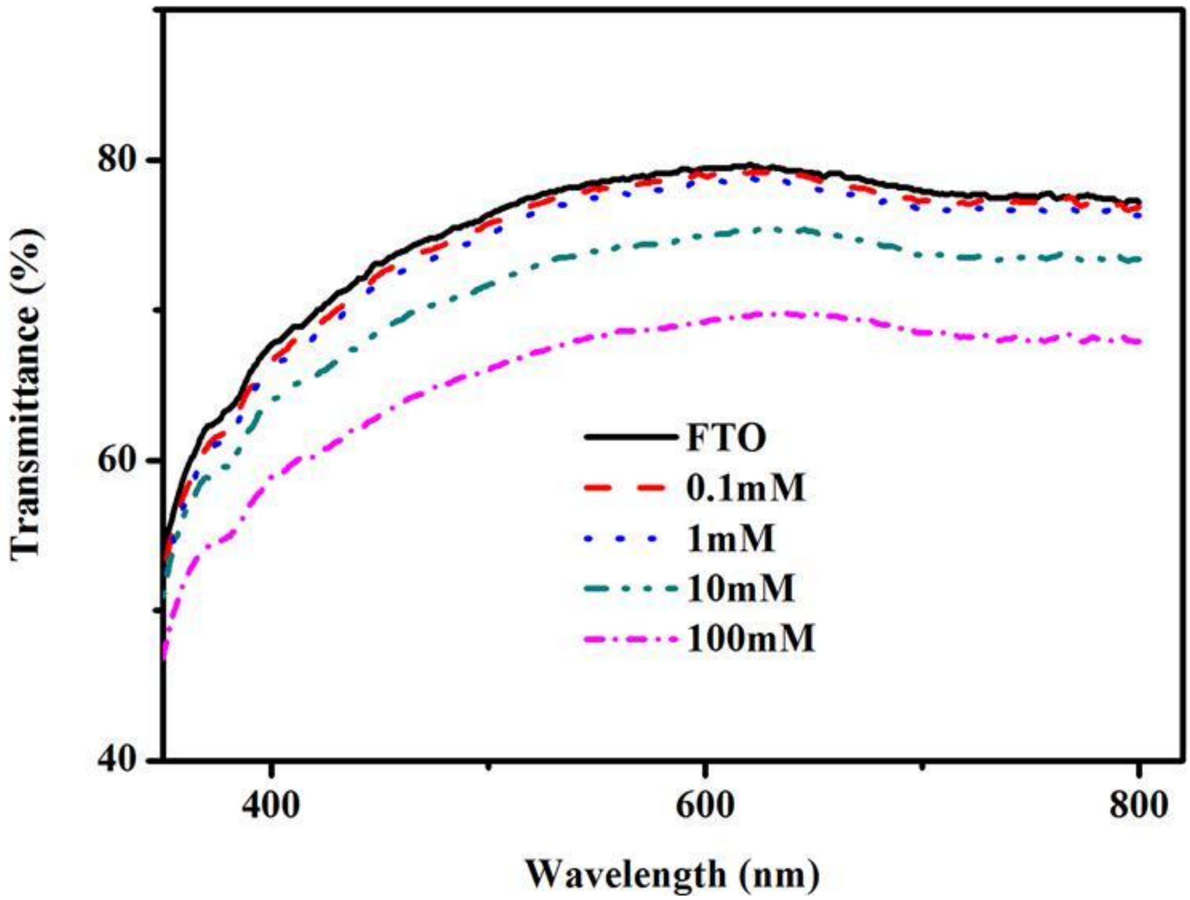

Figure S9. Transmittance change of Pt CEs prepared at the different concentrations of Pt precursor solution with respect to wavelength.

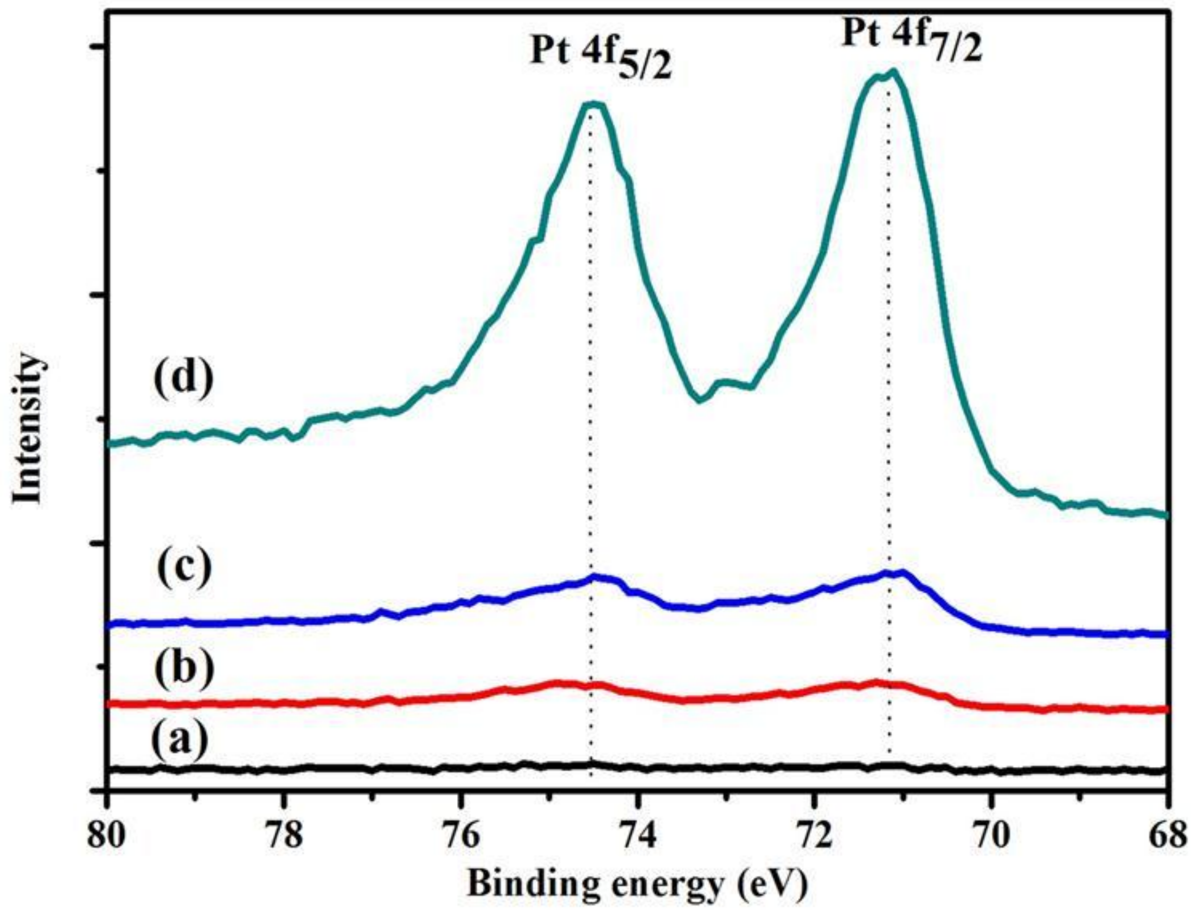

Figure S10. XPS spectra of Pt-NPs/FTO hybrid prepared with various $H_2PtCl_6.xH_2O$ concentrations of (a) 0.1 mM, (b) 1.0 mM, (c) 10mM, and (d) 100 mM in isopropyl alcohol.

Table S8. Percentage of elemental composition on the surface of FTO glass.

	Elemental Composition (%)		
Sample	O	Pt	Cl
(a)	98.83	1.17	0.00
(b)	95.91	4.09	0.00
(c)	80.29	19.71	0.00
(d)	75.38	24.62	0.00

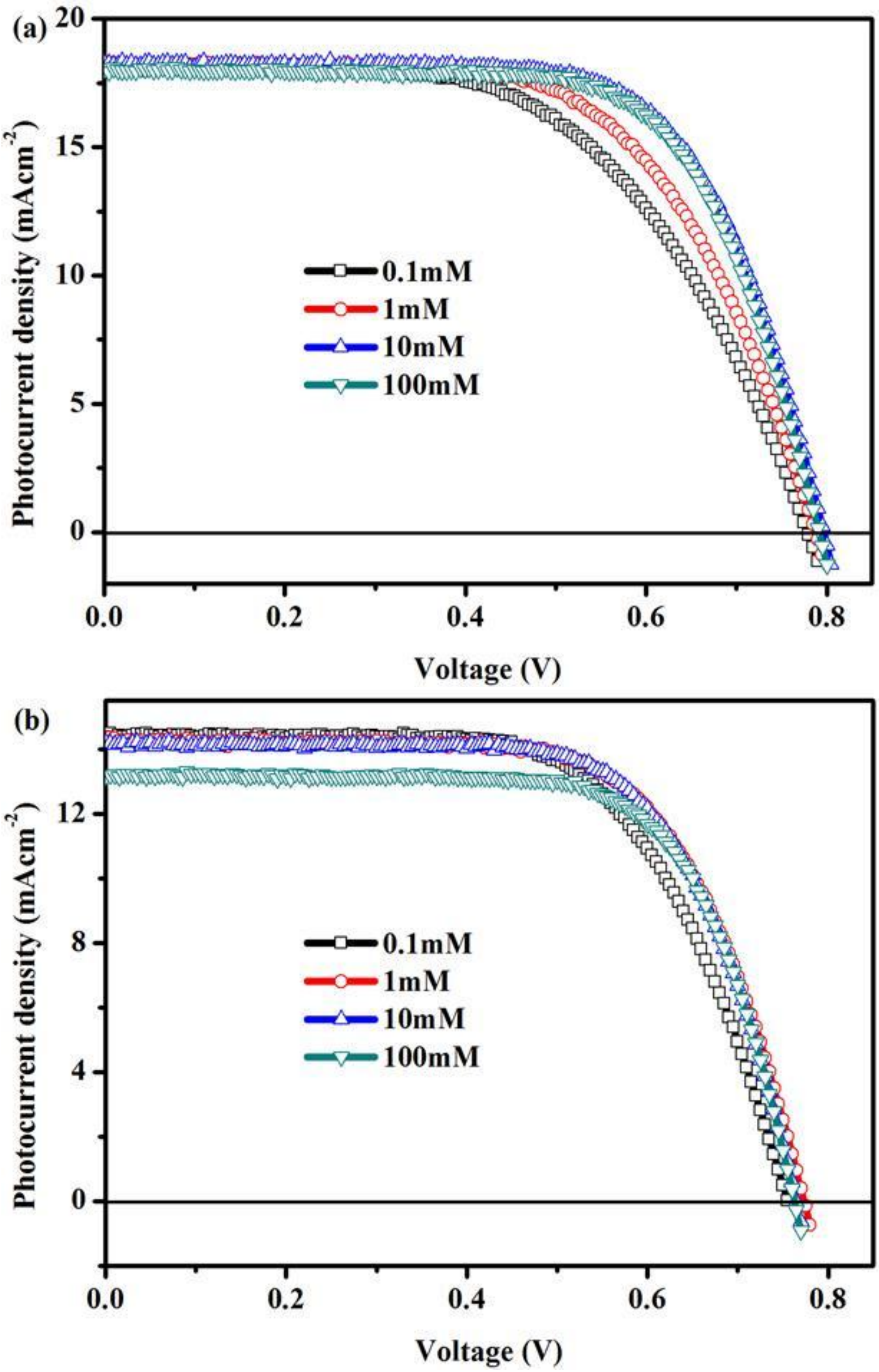

Figure S11. Current-voltage characteristics of four DSCs equipped with Pt-NPs/FTO hybrid electrodes synthesized at four different precursor concentrations; a) PA-side illumination, and b) CE-side illumination. The inset shows the relationships of the conversion efficiency of DSCs with concentration of Pt precursor solution.

Table S9. Photoelectric performances of four DSCs equipped with Pt-NPs/FTO hybrid electrode.

Counter electrode	J_{sc} ($mAcm^{-2}$)	V_{oc} (mV)	FF (%)	η (%)
0.1mM [a]	17.78±0.47	772.50±6.45	57.59±0.74	7.91±0.18
0.1mM [b]	14.40±0.06	753.75±10.31	64.03±1.22	6.91±0.12
1mM [a]	18.14±0.61	782.50±6.45	60.98±2.17	8.65±0.17
1mM [b]	14.60±0.21	766.32±10.77	65.32±0.77	7.31±0.14
10mM [a]	18.48±0.25	795.00±4.08	67.27±0.83	9.88±0.12
10mM [b]	14.00±0.35	772.50±11.90	69.66±1.23	7.53±0.17
100mM [a]	18.55±0.40	785.00±12.91	67.59±0.78	9.84±0.13
100mM [b]	12.76±0.50	757.50±11.90	70.45±0.27	6.81±0.25

[a] photoelectric performance with PA-side illumination

[b] photoelectric performance with CE-side illumination

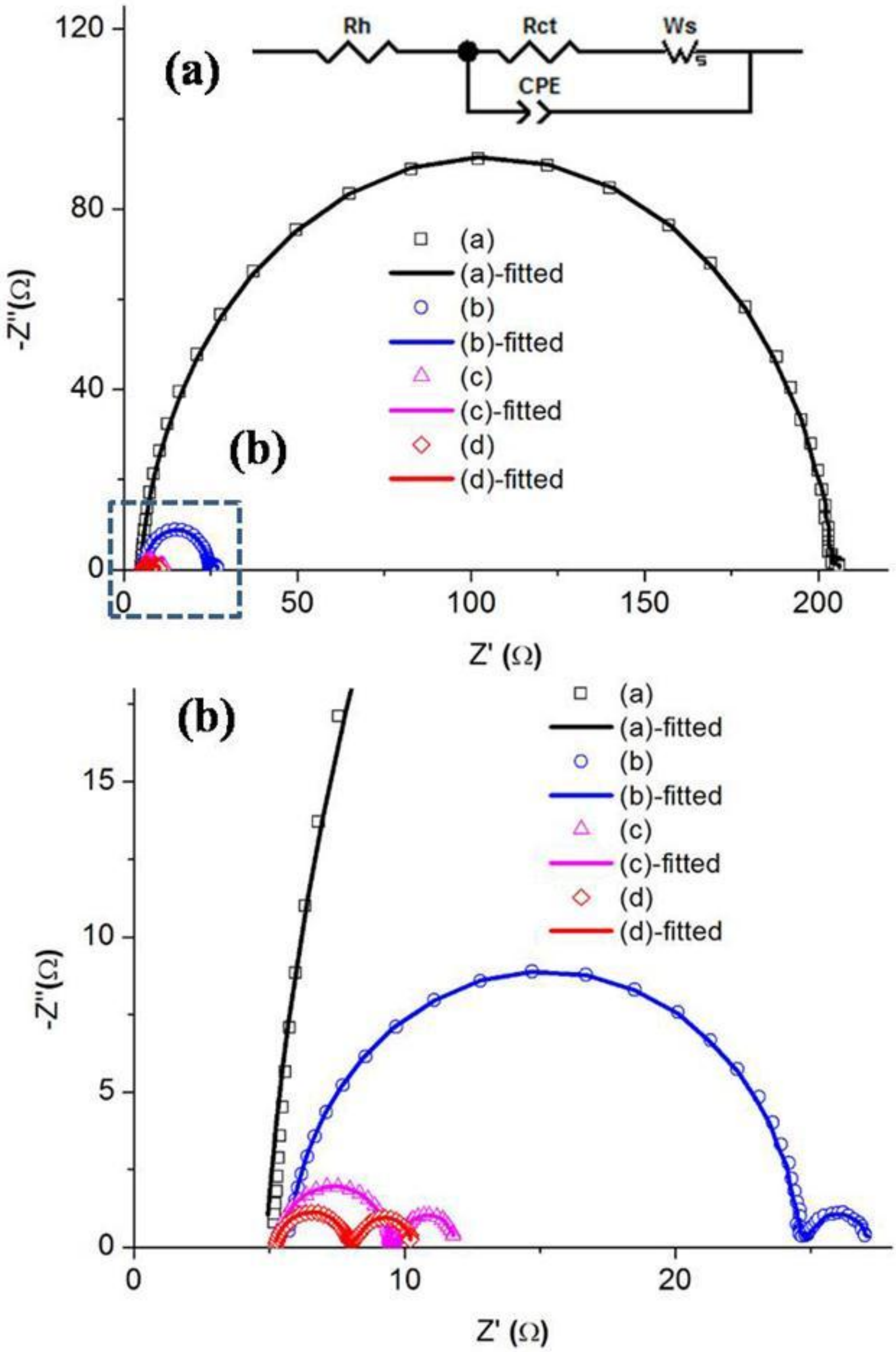

Figure S12. (a) Nyquist plots of the dummy cells fabricated with two identical Pt-NPs/FTO hybrids prepared with Pt precursor solutions containing different concentrations of Pt precursor, and (b) high magnification plots of the square area in (a). The top image shows the equivalent circuit diagram used to fit the observed impedance spectra in this figure. R_h: ohmic serial resistance; Rct: charge-transfer resistance of the counter electrode; CPE: constant-phase element of the counter electrode, and Ws: Warburg impedance.

Table S10. Impedance parameters of the dummy cells fabricated with two identical Pt CEs prepared with Pt precursor solution containing different concentrations of Pt precursor estimated from the impedance spectra and equivalent circuit shown in Fig. S12.

Counter electrode	Rh (Ωcm^2)	Rct (Ωcm^2)	CPE-T (Fcm^{-2})	CPE-P	Ws		
					R	T	P
(a)-0.1mM	1.20	48.68	$1.27x10^{-5}$	0.96	0.63	0.93	0.5
(b)-1mM	1.40	4.61	$1.63x10^{-5}$	0.96	0.63	0.68	0.5
(c)-10mM	1.30	1.01	$2.65x10^{-5}$	0.96	0.61	0.73	0.5
(d)-100mM	1.27	0.67	$14.0x10^{-5}$	0.90	0.57	0.51	0.5

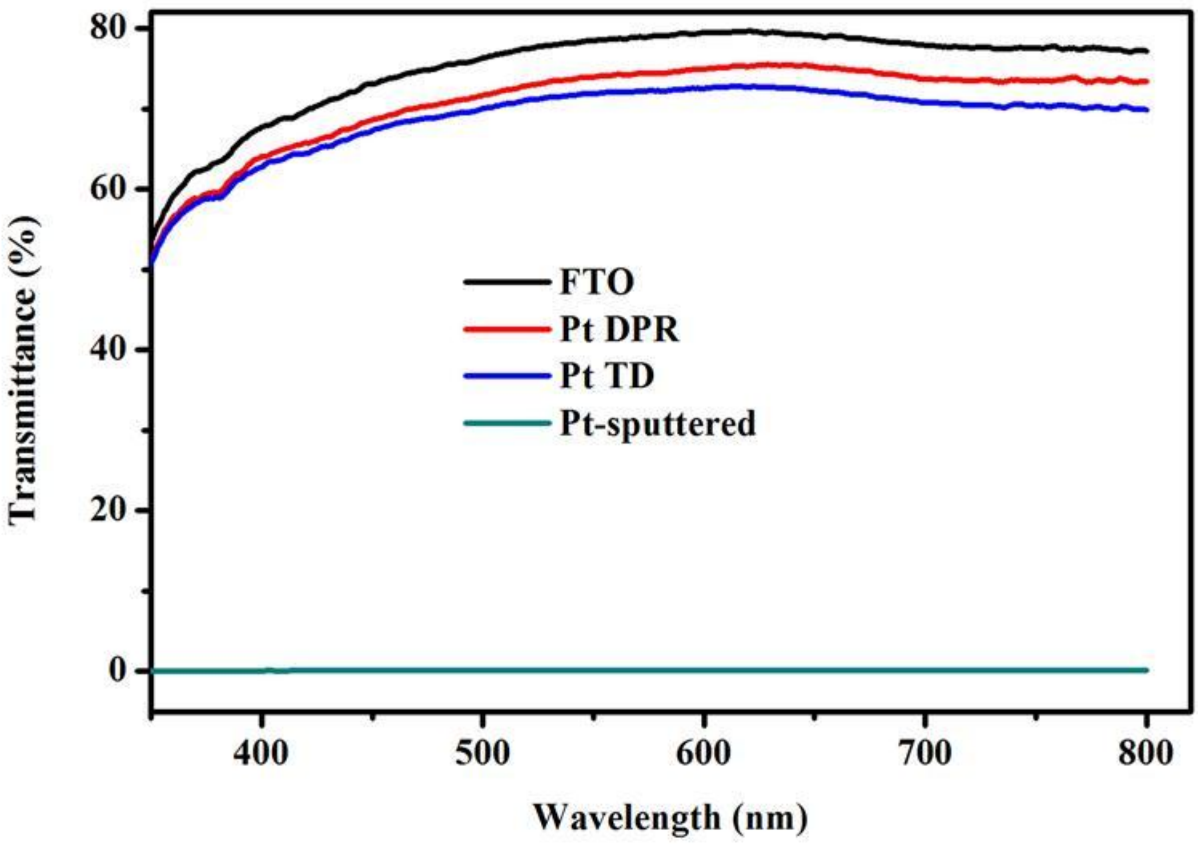

Figure S13. Transmittance change of Pt CEs prepared through DPR, TD, and sputtering with respect to wavelength.

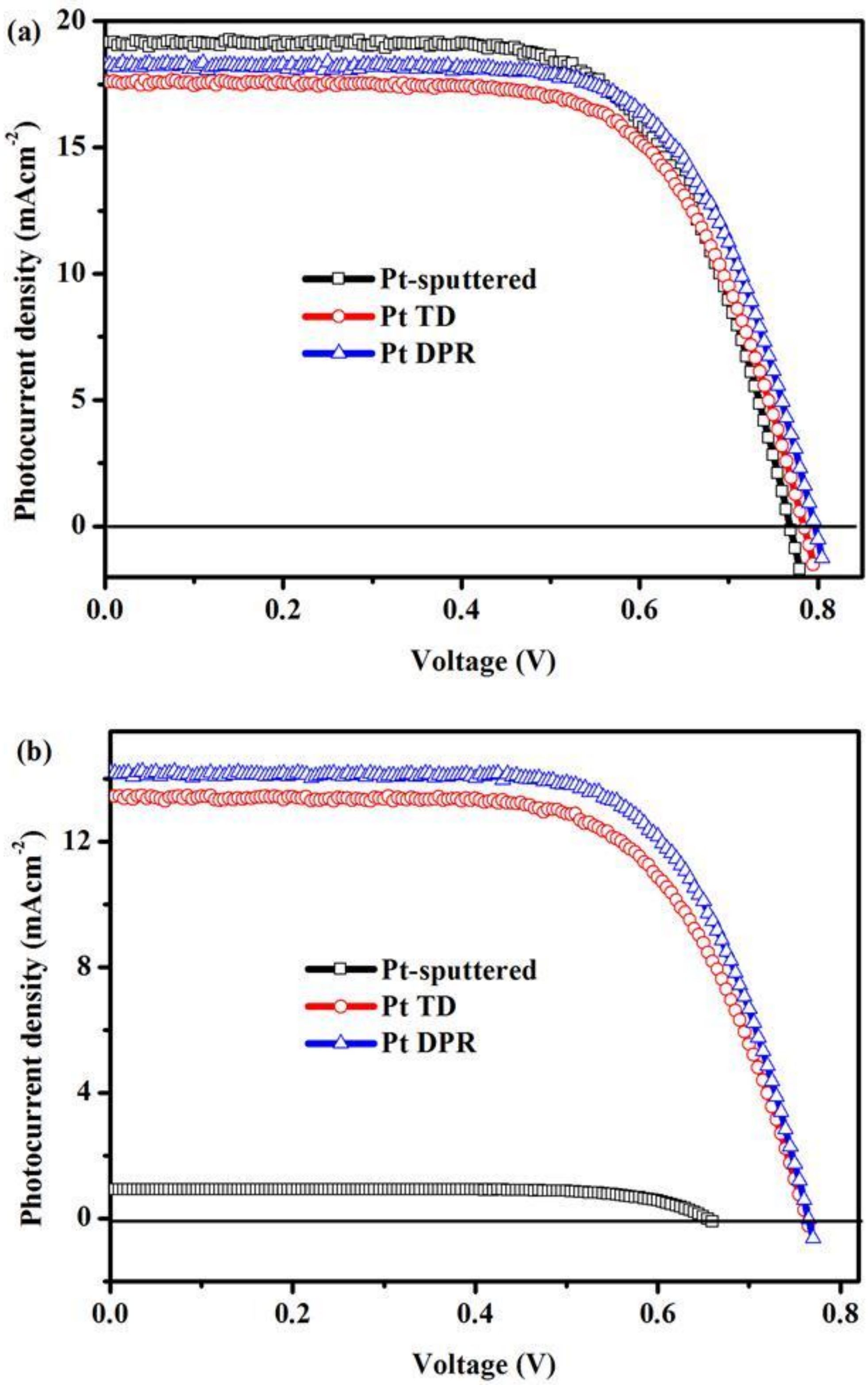

Figure S14. Current-voltage characteristics of three DSCs equipped with Pt-based FTO counter electrodes prepared through three different methods; a) PA-side illumination, and b) CE-side illumination.

Table S11. Photoelectric performances of three cells in Figure S14.

Counter electrode	J_{sc} (mAcm^{-2})	V_{oc} (mV)	FF (%)	η (%)
Pt-sputtered [a]	19.16±0.10	775.00±7.07	66.72±0.73	9.91±0.15
Pt-sputtered [b]	0.93±0.10	637.5±11.9	71.32±2.23	0.42±0.05
Pt-TD[a]	17.69±0.23	778.75±7.50	65.76±1.08	9.06±0.23
Pt-TD[b]	13.26±0.67	756.25±8.53	67.40±2.73	6.75±0.19
Pt-DPR[a]	18.48±0.25	795.00±4.08	67.27±0.83	9.88±0.12
Pt-DPR[b]	14.00±0.35	772.5±11.9	69.66±1.23	7.53±0.17

[a] photoelectric performance with PA-side illumination

[b] photoelectric performance with CE-side illumination

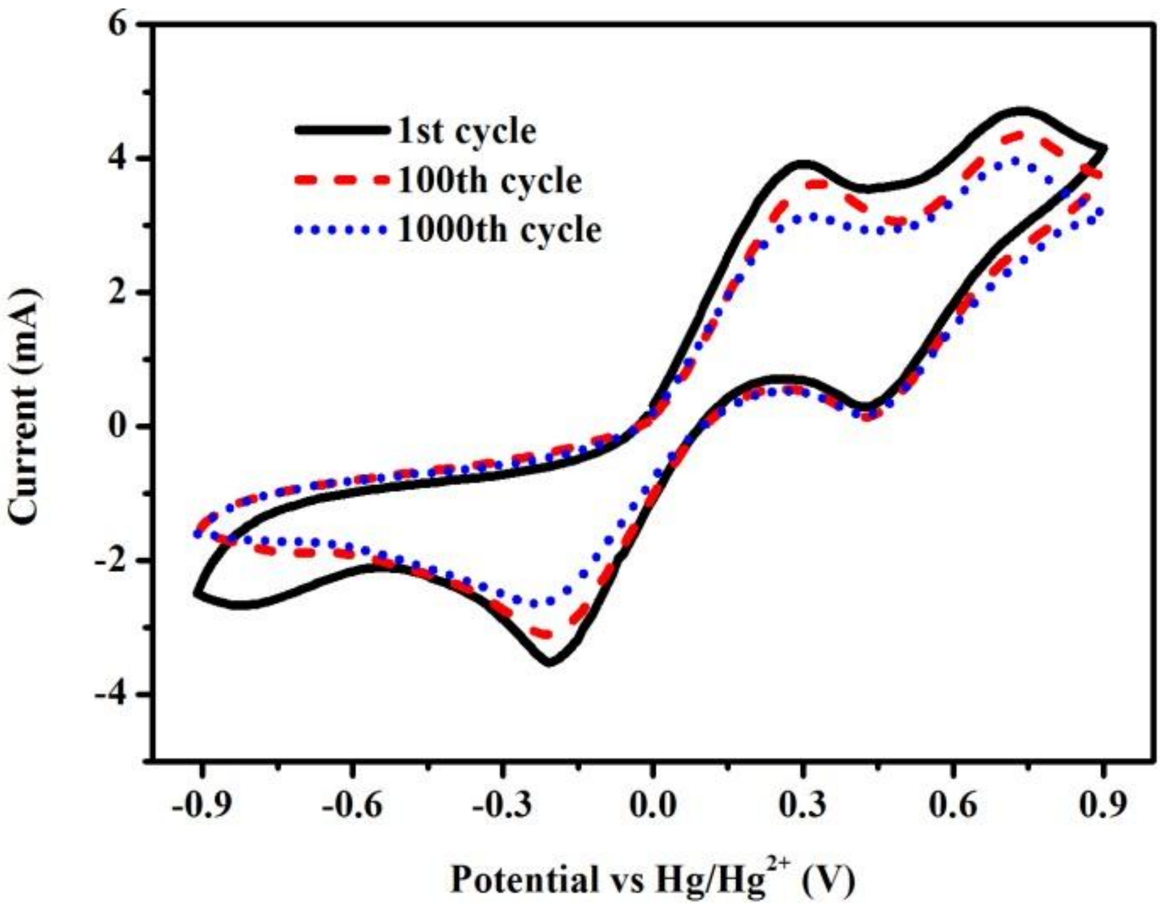

Figure S15. Current-voltage curves over time for the redox system with the Pt NPs working electrode prepared by dry plasma reduction from 10mM of Pt precursor in IPA and Pt-mesh counter electrode.

The stability of the electrode materials is very important for applications. The DSC with the Pt NP as counter electrode prepared by dry plasma reduction showed good stability. This stability was confirmed by the stability of the current-voltage curves over time for the redox system with the Pt NP working electrode and Pt mesh counter electrode (Figure S15) [S1]. Slight decrease of the current was observed after the 1000th cycle. It is, however, better than that of Pt counter electrode prepared by thermal decomposition [S2].

Table S12. Impedance parameters of three DSCs with Pt CEs prepared by sputtering, TD, and DPR, estimated from the impedance spectra and equivalent circuit shown in Figure 3(c).

Counter electrode	R_h (Ωcm^2)	R_{ct1} (Ωcm^2)	CPE1-T (Fcm^{-2})	CPE1-P	R_{ct2} (Ωcm^2)	Ws			CPE2-T (Fcm^{-2})	CPE2-P
						R	*T*	*P*		
Pt-sputtered	1.60	0.72	$1.52x10^{-5}$	0.83	3.14	2.08	0.47	0.5	$7.55x10^{-3}$	0.92
Pt-TD	2.34	1.02	$4.37x10^{-5}$	0.91	3.30	1.86	0.44	0.5	$7.76x10^{-3}$	0.90
Pt-DPR	2.38	0.68	$5.24x10^{-5}$	0.92	2.93	2.30	0.49	0.5	$6.33x10^{-3}$	0.92

Electronic Supplementary Material (ESI) for Journal of Materials Chemistry A

Table S13. Water contact angle of bare FTO glass and PET/ITO substrate before and after plasma treatment.

Substrate	Contact angle	image
FTO-glass	33.6 ± 0.4	
ITO-PET before plasma treatment	94.3 ± 0.2	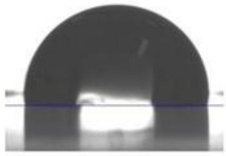
ITO-PET after plasma treatment	15.2 ± 0.4	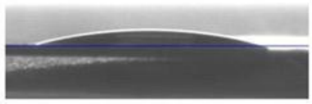

References

[S1] V. D. Dao, S. H. Ko, H. S. Choi, J. K Lee, *J. Mater. Chem.*, 2012, **22**, 14023

[S2] X. Mei, S. Cho, B. Fan and J. Ouyang, *Nanotechnology*, 2010, **21**, 395202